RESEARCH/REVIEW ARTICLE

Turbulent fluxes of momentum and heat over land in the High-Arctic summer: the influence of observation techniques

Anna Sjöblom[1,2]

[1] Department of Earth Sciences, Uppsala University, Villavägen 16, SE-752 36 Uppsala, Sweden
[2] Department of Arctic Geophysics, The University Centre in Svalbard, P.O. Box 156, NO-9171, Longyearbyen, Norway

Keywords
Turbulent fluxes; Svalbard; Arctic; observation techniques; surface energy budget.

Correspondence
Anna Sjöblom, Department of Earth Sciences, Uppsala University, Villavägen 16, SE-752 36 Uppsala, Sweden.
E-mail: anna.sjoblom@geo.uu.se

Abstract

Different observation techniques for atmospheric turbulent fluxes of momentum and sensible heat were tested in a High-Arctic valley in Svalbard during two consecutive summers (June–August in 2010 and 2011). The gradient method (GM) and the bulk method (BM) have been compared to the more direct eddy covariance method (ECM) in order to evaluate if relatively robust and cheap instrumentation with low power consumption can be used as a means to increase the number of observations, especially at remote locations where instruments need to be left unattended for extended periods. Such campaigns increase knowledge about the snow-free surface exchange processes, an area which is relatively little investigated compared to snow-covered ground. The GM agreed closely to the ECM, especially for momentum flux where the two methods agree within 5%. For sensible heat flux, the GM produces, on average, approximately 40% lower values for unstable stratification and 67% lower for stable stratification. However, this corresponds to only 20 and 12 W m^{-2}, respectively. The BM, however, shows a greater scatter and larger differences for both parameters. In addition to testing these methods, radiation properties were measured and the surface albedo was found to increase through the summer, from approximately 0.1 to 0.2. The surface energy budget shows that the sensible heat flux is usually directed upwards for the whole summer, while the latent heat flux is upwards in June, but becomes downward in July and August.

The High Arctic plays a significant role in the Earth's climate system and global climate models project that most of the warming is likely to happen in the polar regions (e.g., Symon et al. 2005; Førland et al. 2011; Walsh et al. 2011). This has implications for, among other things, glacier and sea-ice retreat, permafrost and for humans and other biological systems (e.g., AMAP 2011; Wang & Overland 2012). However, both numerical weather forecast models and global climate models show a high degree of uncertainty in the Arctic (e.g., Overland et al. 2011). To improve the results, a more thorough understanding of the small-scale and surface processes, such as radiation properties, turbulent exchange processes of momentum and heat and the surface energy budget (SEB) is essential. More observations are therefore vital.

Taking meteorological observations in the High Arctic is generally challenging and most measuring campaigns in remote parts of this region are over very short periods—perhaps only days or weeks—due to logistical limitations. There are some longer campaigns, for example, the Surface Heat Budget of the Arctic Ocean (SHEBA) Experiment (e.g., Persson et al. 2002; Grachev et al. 2007, 2008), in which the atmospheric boundary layer and the SEB were studied over sea ice for a whole year, but these are few in number. The SEB has also been investigated over land, for example, in Siberia (Langer et al. 2011), Alaska (McFadden et al. 1998; Lynch et al. 1999), Canada (Ohmura 1982), Greenland (Rott & Obleitner 1992; Duynkerke & van den Broeke 1994) and sub-Arctic areas (Eugster et al. 2000).

Citation: *Polar Research* 2014, *33*, 21567, http://dx.doi.org/10.3402/polar.v33.21567

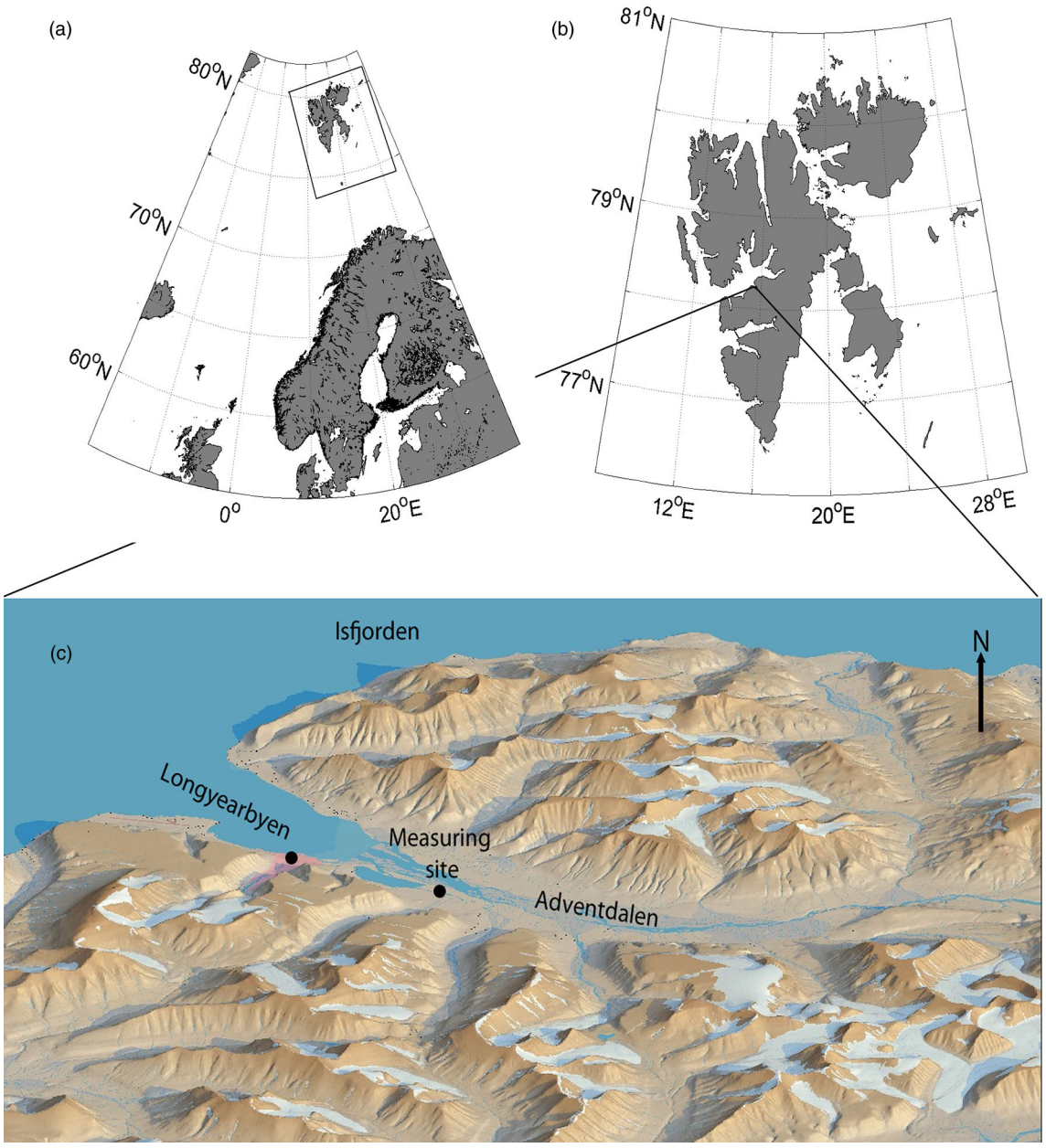

Fig. 1 (a) The archipelago of Svalbard north of mainland Norway. (b) The location of Adventdalen on the island of Spitsbergen. (c) The measuring site (image published courtesy of the Norwegian Polar Institute).

Studies of small-scale meteorological processes and surface exchange process have been made over land in Svalbard, an archipelago about 700 km north of the Norwegian mainland, with underlying permafrost and approximately 60% of its surface covered with permanent snow and ice (Fig. 1). For example, Westermann et al. (2009) studied the SEB for a year in Svalbard, Boike et al. (2003) focused on the snow covered period, Harding & Lloyd (1998) looked at the SEB for two summers and Lloyd et al. (2001) compared energy and water fluxes from Svalbard with three other sites in the European Arctic. Meteorological interest in Svalbard has increased significantly in recent years, as shown by the rising publication rate on this subject (Esau et al. 2012). However, previous studies suggest that small-scale processes here are very local and that spatial variation is significant (e.g., Sjöblom 2010; Kilpeläinen et al. 2011; Westermann et al. 2011; Kral et al. 2014). Therefore, questions remain concerning how many generalizations can be drawn, even in a small area, and what drives these local processes.

Citation: *Polar Research* 2014, *33*, 21567, http://dx.doi.org/10.3402/polar.v33.21567

Moreover, most earlier studies over land in polar regions have focused on the snow-covered period and relatively little is known about similar processes in the summer. Are these processes comparable to processes at lower latitudes and do summer processes have the same spatial variability as in winter? In a warming climate with longer snow-free periods, these questions become increasingly important, for example, for thawing of the permafrost, environmental conditions for plants and animals (Eugster et al. 2000; Ávila-Jiménez et al. 2010).

A problem with ensuring high-quality observations is that the instruments usually require regular maintenance, which limits study areas and length of the measuring campaigns. Despite the rigorous conditions, it is in some ways easier to take measurements over land in the High Arctic during the winter than in the summer since snowmobiles can be used to move around in the terrain. Since there are very few roads, summer study areas usually have to be restricted to the vicinity of settlements or to areas easily accessed by ship or helicopter. The alternative is to use observation techniques and robust instrumentation that can be established in remote areas during the winter and left unattended for a longer time.

There are several methods to determine turbulent fluxes of momentum and sensible heat. Each method is dependent on the instrumentation available and how great an accuracy is required. All of them have their own advantages and disadvantages. The preferred technique is the eddy covariance method (ECM), which is often considered to be the most accurate method and is normally used as a reference when other methods are evaluated. However, the ECM requires a stable platform and is, in addition, very sensitive to flow distortion. This method also requires fast-response turbulence measurements recorded with relatively delicate instrumentation and a stable power supply. The alternative is to use the gradient method (GM) or the bulk method (BM). In the GM, observations at two arbitrary levels are necessary while the BM requires only one level of meteorological instrumentation (usually 10 m) in addition to surface values. Both techniques can be applied with robust slow-response instruments which have a smaller power requirement and which can be left unattended for longer periods at remote locations.

However, the level of confidence that can be placed in the GM and the BM is unclear. Can these techniques be used as a means to increase the number of observations in the High Arctic? The BM is often used in polar regions, particularly over water and sea ice, and the parameterization has been investigated during several campaigns (e.g., Brunke et al. 2006; Andreas, Horst et al. 2010; Andreas, Persson et al. 2010; Lüpkes et al. 2012). Lüers & Bareiss (2010) tested the BM in Ny-Ålesund over land in the winter and concluded that the fundamental surface parameters can be difficult to determine, in addition to further problems determining the temperature profiles close to the ground over snow. This results in potentially wide errors in the calculated fluxes. To the knowledge of this author, there has not been a similar investigation of either the accuracy of the BM or the GM in the snow-free summer over land in the Arctic.

The two methods—BM and GM—were therefore assessed and compared to the ECM during two summers in Adventdalen (Fig. 1), a large High-Arctic valley in Svalbard. This type of data is rare, not only because they were taken in the snow-free period, but also since it was possible to use three different observation techniques simultaneously. In addition to presenting a comparison of the different methods, this study calculates the radiation budget, the albedo (α) and the SEB. The challenges associated with determining the aerodynamic roughness length (z_0) are also discussed.

Theory

Radiation fluxes and albedo

The radiation budget can be described as:

$$R_N = S_{in} - S_{ref} + L_{in} - L_{out}, \quad (1)$$

where R_N is the net radiation (W m^{-2}), S_{in} the incoming shortwave radiation (W m^{-2}), S_{ref} the reflected shortwave radiation (W m^{-2}), L_{in} the incoming longwave radiation (W m^{-2}) and L_{out} the outgoing longwave radiation (W m^{-2}). R_N is defined as positive downwards, that is, when the radiation contributes to the heating of the surface. The albedo, α, is defined as:

$$\alpha = S_{ref}/S_{in} \quad (2)$$

L_{out} can also be used to determine the surface temperature, θ_0 (K), through Stefan-Boltzmann's law:

$$L_{out} = \varepsilon\sigma\theta_0^4, \quad (3)$$

where ε is the emissivity and σ the Stefan-Boltzmann constant (W m^{-2} K^{-4}).

Atmospheric stratification

Turbulent fluxes are dependent on the atmospheric stratification (also called stability), which can be quantified through, for example, the gradient Richardson number, *Ri*:

$$Ri = \frac{g}{T_0}\frac{\partial\theta/\partial z}{(\partial U/\partial z)^2}, \quad (4)$$

where g is acceleration due to gravity (m s^{-2}), T_0 a reference temperature for the surface layer (K; often the temperature at 2 m is applied), $\partial\theta/\partial z$ the potential temperature gradient (K m^{-1}) and $\partial U/\partial z$ the wind speed gradient (s^{-1}). $Ri>0$ indicates a stable stratification, $Ri<0$ unstable stratification and $Ri=0$ neutral stratification. Instead of using gradients as in Eqn. 4, the bulk Richardson number Ri_B can be used as an alternative with finite differences of potential temperature, θ (K), wind speed, U (m s^{-1}) and measuring height (z):

$$Ri_B = \frac{g}{T_0}\frac{\Delta\theta\Delta z}{(\Delta U)^2} \tag{5}$$

Stability can also be described through the so-called Obukhov length, L, and the non-dimensional parameter z/L:

$$\frac{z}{L} = -\frac{zgk\overline{w'\theta'_v}}{u_*^3 T_0} \tag{6}$$

Here, k is the von Karman constant, set to 0.40 (Högström 1996). $\overline{w'\theta'_v}$ is the virtual kinematic heat flux (m K s^{-1}) and u_* the friction velocity (m s^{-1}); according to Monin-Obukhov similarity theory (e.g., Obukhov 1971), both can be assumed constant in the surface layer. u_* is linked to the momentum flux or stress, τ (N m^{-2}), through

$$|\tau| = \rho\left(\overline{u'w'}^2 + \overline{v'w'}^2\right)^{1/2} = \rho u_*^2, \tag{7}$$

where ρ is the density of air (kg m^{-3}) and $\overline{u'w'}$ and $\overline{v'w'}$ (m^2 s^{-2}) are the vertical stress components along and across the average wind.

Ri and z/L are connected, but there are different suggestions regarding the exact relation. For stable conditions ($0 \le Ri \le 0.2$)

$$\frac{z}{L} = \frac{Ri}{1-5Ri} \tag{8}$$

is often suggested (Arya 2001), while for unstable conditions, there are mainly two proposals, Arya (2001):

$$Ri \approx z/L \tag{9}$$

or Högström (1996):

$$Ri \approx 1.5z/L \tag{10}$$

Both are valid for at least $-z/L<0.5$.

Roughness

The roughness length, z_0 (m), is defined as the height above the surface at which the wind speed is zero and is logarithmically dependent on the surface type and the height of the vegetation, obstacles, etc. Through the logarithmic wind law (e.g., Arya 2001) and assuming neutral stratification, it can be calculated as:

$$z_0 = \frac{z}{e^{(kU/u_*)}} \tag{11}$$

However, this method uses u_*, which usually requires fast-response turbulence measurements to determine. If wind speed measurements with slow-response instruments are available at two levels (1 and 2), Eqn. 11 can be simplified since u_* is assumed to be constant in the surface layer. Hence:

$$\ln z_0 = \left(\frac{U_1 \ln z_2 - U_2 \ln z_1}{U_1 - U_2}\right) \tag{12}$$

The equivalent roughness length for temperature, z_{0T}, is often suggested to be 10% of z_0 (Foken 2008).

Turbulent fluxes of momentum and heat

As discussed earlier in this paper, several observation techniques are available to determine the turbulent fluxes from measurements. The three used here are described below.

Eddy covariance method. By utilizing direct fast-response turbulence measurements, τ can be determined directly through Eqn. 7, and the sensible heat flux, H_S (W m^{-2}), defined as positive upwards:

$$H_S = \rho c_p \overline{w'\theta'}, \tag{13}$$

in which $\overline{w'\theta'}$ is the kinematic heat flux (m K s^{-1}) and c_p the heat capacity of air (J kg^{-1} K^{-1}). Most fast-response turbulence instruments measure the so-called sonic temperature, which is close—about 0.20%—to the virtual temperature (Sjöblom & Smedman 2002), so instead of $\overline{w'\theta'}$, $\overline{w'\theta'_v}$ is measured. Following Lumley & Panofsky (1964) the two fluxes are connected:

$$\overline{w'\theta'} = \frac{\overline{w'\theta'_v}}{1+(0.07/B)}, \tag{14}$$

where B is the Bowen ratio, that is, the ratio between H_S and the latent heat flux, H_L (W m^{-2}). Great accuracy of B is usually not needed for this correction and can, for example, be determined as $c_p\Delta\theta/L_e\Delta q$ using slow-response instruments, where L_e is the latent heat of evaporation (J kg^{-1}) and q the specific humidity (kg kg^{-1}).

Citation: *Polar Research* 2014, *33*, 21567, http://dx.doi.org/10.3402/polar.v33.21567

Gradient method. The method only requires slow-response measurements of U and θ, at two arbitrary levels, that is, τ and H_S can be determined as:

$$\tau = \rho\left[\frac{k\Delta U}{\phi_m[\ln(z_2/z_1)]}\right]^2 \quad (15)$$

$$H_s = -\rho c_p\left[\frac{k^2\Delta U\Delta\theta}{\phi_m\phi_h[\ln(z_2/z_1)]^2}\right], \quad (16)$$

where ϕ_m and ϕ_h are the non-dimensional gradients of wind speed and temperature, respectively (Högström 1996):

$$\phi_m = (1 - 19z/L)^{-1/4} \quad (17)$$

$$\phi_h = 0.95(1 - 11.6z/L)^{-1/2}, \quad (18)$$

which are valid for unstable conditions (at least for $-2.0 < z/L < 0$). For stable conditions ($0 < z/L < 0.5$), Högström (1996) recommends:

$$\phi_m = 1 + 5.3z/L \quad (19)$$

$$\phi_h = 1 + 8.0z/L \quad (20)$$

H_L can also be determined in a similar manner with q from two measuring levels:

$$H_L = -\rho L_e\left[\frac{k^2\Delta U\Delta q}{\phi_m\phi_q[\ln(z_2/z_1)]^2}\right], \quad (21)$$

where ϕ_q is the non-dimensional gradient for specific humidity (usually assumed to be similar to ϕ_h).

Bulk method. Only one level of U and θ is needed in this observation technique; traditionally that height is 10 m, although other levels are used as well, especially in numerical models. In addition, measurements of θ_0, usually through measurements of L_{out} (Eqn. 3), are required. τ and H_S are then determined as:

$$\tau = \rho C_D U_{10}^2 \quad (22)$$

$$H_S = -\rho c_p C_H U_{10}(\theta_{10} - \theta_0), \quad (23)$$

where U_{10} is the wind speed at 10 m (m s^{-1}) and θ_{10} the potential temperature at 10 m (K). C_D and C_H are the drag coefficient and the Stanton number, respectively, defined as:

$$C_D = \left(\frac{u_*}{U_{10}}\right)^2 = k^2\left[\ln\frac{z}{z_0} - \psi_m\left(\frac{z}{L}\right)\right]^{-2} \quad (24)$$

$$C_H = \frac{\overline{w'\theta'}}{U_{10}(\theta_0 - \theta_{10})} = k^2\left[\ln\frac{z}{z_0} - \psi_m\left(\frac{z}{L}\right)\right]^{-1}\left[\ln\frac{z}{z_T} - \psi_h\left(\frac{z}{L}\right)\right]^{-1}, \quad (25)$$

where ψ_m and ψ_h are the integrated ϕ-functions (Eqns. 17–20), which, according to Paulson (1970) and Högström (1996), can be calculated as:

$$\psi_m = 2\ln[(1 + \phi_m)/2] + \ln\left[\left(1 + \phi_m^2\right)/2\right] - 2\tan^{-1}\phi_m + \pi/2 \quad (26)$$

$$\psi_h = 2\ln\left[\left(1 + \phi_h^2\right)/2\right] \quad (27)$$

for $z/L < 0$, and for $z/L > 0$:

$$\psi_m = -5.3z/L \quad (28)$$

$$\psi_h = -8.0z/L \quad (29)$$

If temperature and wind speed measurements are taken at heights other than 10 m, the data have to be re-calculated to fit 10 m first.

Surface energy budget

The SEB is defined as:

$$R_N = H_s + H_L + H_G, \quad (30)$$

where R_N is calculated by Eqn. 1. H_G is the ground heat flux (W m^{-2}), positive when the energy goes into the ground. If H_G cannot be measured directly, it is often determined as a residual if the other terms in Eqn. 30 are known.

Observations and data handling

The observations were taken in Adventdalen (N 78° 12′ 10″, E 15° 49′ 41″), Svalbard, approximately 4 km south–east of the main settlement, Longyearbyen (Fig. 1), during two consecutive summers, June–August 2010 and 2011. Longyearbyen has midnight sun between 19 April and 23 August, so the sun was above the horizon for the majority of the measuring period. The summer period has a mean air temperature of only +4.2°C, despite the midnight sun, while the mean annual air temperature is −6.6°C (Førland et al. 2011). Adventdalen is a long valley, orientated north–west to south–east, approximately 4 km wide and surrounded by mountains with maximum heights varying between 600 and 900 m. In addition, there are side valleys entering into Adventdalen

(Fig. 1). The wind is usually channelled through Adventdalen, resulting in local winds that are either north-westerly or south-easterly. The measuring site, more than 3 km from the coastline, is situated about 15 m above mean sea level and the ground surface in the valley at the station site is flat tundra with a mixture of bare soil (moist clay or sand) and sparse vegetation (*Luzula* tundra) of a few centimetres in height. Adventdalen has underlying permafrost with an active layer of approximately 1 m, that is, only the uppermost 1 m layer thaws in summer. The amount of precipitation in Adventdalen is generally low; the average for the town of Longyearbyen is approximately 200 mm per year, with about 50 mm in the period June–August (Førland et al. 2011). This low yearly precipitation also means that the snow depth is relatively small in winter and that the ground usually begins to become snow-free in May, which is early compared to other places in Svalbard.

Slow-response measurements of wind speed, wind direction, temperature and relative humidity were taken at two heights (wind speed and wind direction at 2.1 m and 10.1 m; temperature and relative humidity at 2.1 and 9.1 m), all measuring at 1 Hz. Wind speed and wind direction were measured with a model 05103-45 Alpine Wind Monitor (accuracy ± 0.3 m s^{-1} or 1%; R.M. Young Co., Traverse, MI, USA), temperature with a naturally ventilated model 41342 Platinum Temperature Probe (accuracy $\pm 0.1^{\circ}$; R.M. Young Co.) and relative humidity with a HygroClip (accuracy $\pm 1.5\%$ at 23°C; Rotronic Instrument Corp., Hauppauge, NY, USA). In addition, a CSAT3 Sonic Anemometer (Campbell Scientific, Logan, UT, USA), measuring at 20 Hz, was installed on a separate tower (at 2.8 m in 2010 and 2.7 m in 2011) about 40 m from the slow-response instrument tower. Radiation was measured (averaging time of 5 min) at the site using a CNR-1 Net Radiometer (no heating applied and expected accuracy for daily totals: $\pm 10\%$; Kipp & Zonen, Delft, The Netherlands). All the instruments were regularly checked, including standard maintenance of the sonic anemometer and the radiometer. Moreover, no frost or dew was ever observed on the radiometers domes.

The data were thoroughly quality assured manually before averaging into 30-min means and removing potentially disturbed and non-stationary data. This included, for example, non-consistent wind directions, large temperature changes and data collected when the wind was coming from the river behind the station. Hence, the fetch can be considered homogeneous in all directions used, and for the current observation heights, no internal boundary layers were expected to build up which could influence the results. Only data with $U > 2$ m s^{-1} and a difference between the two measuring levels of 0.1 m s^{-1} were used. For θ the threshold difference between the two levels was set to 0.1°C and for relative humidity 1%. In addition, only sonic anemometer data with $\left|\overline{w'\theta_v'}\right| > 0.005$ K m^{-1} s^{-1} were used for the calculation of H_s. All these limitations were introduced in order to avoid instrument uncertainties at low measuring values. It should, however, be noted that the threshold values chosen are in some cases close to the instrument accuracies specified earlier, which could affect the smallest gradients. Since temperature and relative humidity were measured at 9 m, they were recalculated to 10 m for the BM with a straight profile from measurements at 2 m (or the surface) and 9 m.

The sonic anemometer was corrected for crosswind contamination on-line (e.g., Schotanus et al. 1983) and spike removal according to Vickers & Mahrt (1997) has been applied. The wind components from the sonic anemometer were rotated into a streamwise coordinate system by the double rotation procedure described in Lee et al. (2004).

The slow-response instruments measured between 1 June and 31 August in both 2010 and 2011, with only short interruptions due to technical problems. The sonic anemometer and the radiation instruments were measuring 5 July–31 August in 2010, while in 2011 the period was 1 June–31 August for the radiation instrument and 17 June–31 August for the sonic anemometer. All times are given in UTC, which is 1 h behind local standard time.

Results

An overview of the daily mean meteorological conditions for the two summers is presented in Fig. 2 and monthly means in Table 1. The summer of 2011 was generally warmer than in 2010 with the warmest period in August 2011 and a maximum temperature of 16.4°C at 2 m (T_2). These unusually warm days set new temperature records for August for some locations in Svalbard. Minus degrees only occurred for short periods in June and August 2010. The relative humidity was very similar for both years and was generally high (about 75% on average), which Svalbard's comparatively low temperatures would lead one to expect. However, during the warm period in August 2011, the minimum relative humidity at 2 m (RH_2) was only 25%. On average, the wind speed was low, around 5 m s^{-1} at 10 m (U_{10}) but strong winds over 15 m s^{-1} occurred occasionally in both summers. The snow cover (not shown) started to disappear in mid-May in both years and by the beginning of June only small patches of snow remained.

Citation: *Polar Research* 2014, *33*, 21567, http://dx.doi.org/10.3402/polar.v33.21567

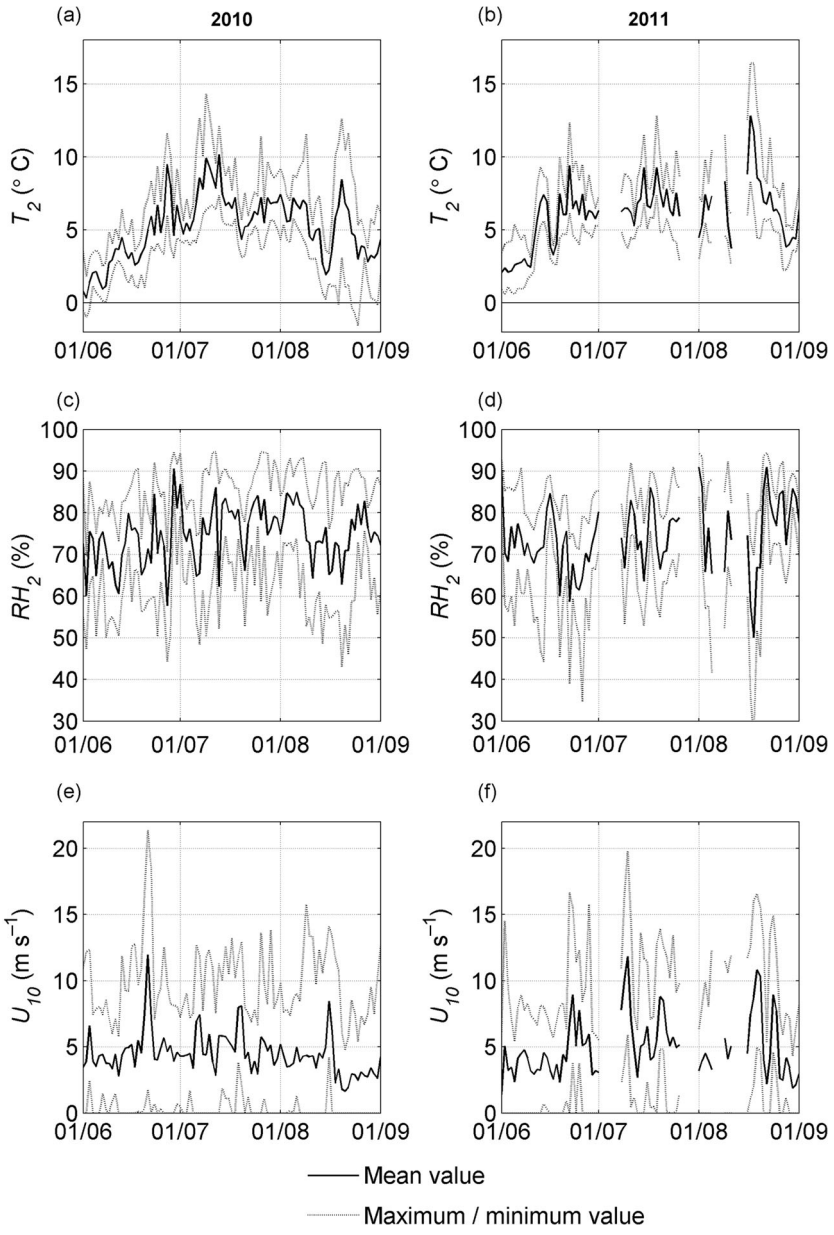

Fig. 2 Overview of daily meteorological parameters: (a) temperature at 2 m (T_2) in 2010 and (b) in 2011; (c) relative humidity at 2 m (RH_2) in 2010 and (d) in 2011; (e) wind speed at 10 m (U_{10}) in 2010 and (f) in 2011.

Radiation fluxes and albedo

Figure 3a and b show the daily means of the four radiation components, S_{in}, S_{ref}, L_{in} and L_{out}, for the two years, respectively. Note that in 2010 the radiation measurements commenced on 5 July. The two years show a similar pattern, with large daily variations in S_{in}. S_{in} is greatest in June and decreases in July and August as the sun angle is reducing and midnight sun finally ends on 23 August. S_{in} in Adventdalen is lower than that Niu et al. (2010) suggested from large-scale satellite measurements in July (approximately 200 W m^{-2}), but corresponds well to measurements in Ny-Ålesund, Svalbard, where Westermann et al. (2009), found an average value of S_{in} of 144 W m^{-2} for July and August. The longwave radiation has only small daily variations and L_{out} is usually larger than L_{in} with average values of approximately 350 and 300 W m^{-2}, respectively. Like the shortwave radiation, the longwave radiation is similar to the findings of Westermann et al. (2009).

Table 1 Monthly overview of mean meteorological parameters at 2 and 10 m: temperature (T_2 and T_{10}), relative humidity (RH_2 and RH_{10}) and wind speed (U_2 and U_{10}); mean sensible heat fluxes from the eddy covariance method ($H_{S,ECM}$), the gradient method ($H_{S,GM}$), the bulk method ($H_{S,BM}$) and the modified bulk method ($H_{S,BM,Mod}$), and mean latent heat flux from the gradient method ($H_{L,GM}$). Numbers in brackets indicate the percentage of data available.

	June		July		August	
	2010	2011	2010	2011	2010	2011
T_2 (°C)	3.7 (100)	4.9 (100)	6.7 (100)	6.9 (65)	5.0 (100)	6.7 (77)
T_{10} (°C)	3.5 (100)	4.7 (100)	6.6 (100)	6.8 (65)	5.0 (100)	6.7 (77)
RH_2 (%)	72 (100)	72 (100)	77 (100)	75 (65)	75 (100)	76 (77)
RH_{10} (%)	73 (100)	72 (100)	79 (100)	76 (65)	77 (100)	77 (77)
U_2 (m s^{-1})	4.1 (100)	3.5 (100)	4.1 (100)	5.0 (65)	3.0 (100)	3.9 (77)
U_{10} (m s^{-1})	4.8 (100)	4.2 (100)	4.9 (100)	6.1 (65)	3.7 (100)	5.0 (100)
$H_{S,ECM}$ (W m^{-2})	–	42.1 (36)	37.6 (60)	24.3 (64)	25.7 (60)	11.0 (67)
$H_{S,GM}$ (W m^{-2})	31.6 (85)	26.0 (86)	27.4 (61)	10.5 (75)	13.9 (64)	−3.1 (67)
$H_{S,BM}$ (W m^{-2})	–	97.5 (79)	109.7 (64)	79.7 (66)	67.9 (69)	54.3 (70)
$H_{S,BM\ Mod}$ (W m^{-2})	–	65.9 (79)	74.6 (64)	54.6 (66)	46.2 (69)	41.8 (70)
$H_{L,GM}$ (W m^{-2})	−3.9 (85)	19.7 (86)	−17.7 (61)	−8.8 (75)	−16.2 (64)	−16.3 (67)

The daily averages of R_N (Eqn. 1) shown in Fig. 3c and d, together with its maximum and minimum values, are also decreasing through the summer as expected. The average R_N is positive during the whole summer for both years, but the variability is great and individual 30-min means can be either twice the average value or negative at any time.

α (Eqn. 2) is presented in Fig. 3e and f (daily averages). α changes from approximately 0.1 in early June to 0.2 later in the summer. An α of 0.1 is close to that found in Ny-Ålesund, Svalbard, just after snowmelt (Harding & Lloyd 1998; Lloyd et al. 2001; Winther at al. 2002), and 0.18 was found at the same location in August by Westermann et al. (2009). However, snowmelt is usually earlier in Adventdalen (late May) than in Ny-Ålesund (late June). Hence, α is increasing faster in Adventdalen, which also suggests that the ground surface is drying faster.

Figure 4 shows the 24-h radiation budget for the three months (hourly means). Since the radiation measurements started late in 2010, Fig. 4a only consists of data from 2011, while Fig. 4b and c contain data from both years. S_{in} has its peak before UTC noon, with a maximum in June in the order of 400 W m^{-2}. Due to the midnight sun, S_{in} never becomes zero, with a minimum in August of about 10 W m^{-2} during the night. L_{in} remains approximately constant through the summer (about 300 W m^{-2}) and hardly any diurnal variation can be observed. L_{out} on the other hand, has a slight increase during the day due to increasing surface temperature. It is also constantly larger than L_{in}. R_N is positive during most of the measuring period and, as also seen in Fig. 3, it is only in August that R_N becomes slightly negative (about −25 W m^{-2}) during the night.

Atmospheric stratification

As described earlier, the stratification can be expressed in several ways. According to Eqns. 8–10, Ri and z/L are correlated and in order to test these relationships, two types of Ri_B were calculated and compared to z/L (Eqn. 6). In Fig. 5a, Ri_B (Eqn. 5) was calculated using measurements at 2 and 10 m ($Ri_{B,2/10}$) and in Fig. 5b using measurements at the surface and 10 m ($Ri_{B,S/10}$). U is assumed to be zero at the surface and θ_0 is calculated from Eqn. 3, using $\varepsilon = 0.97$, in accordance with Arya (2001), an ε for bare soil with moist clay, which resembles the surface at the measuring site in Adventdalen. All three stability estimates indicate close to neutral or slightly unstable stratification most of the time, with the most unstable stratification in June (not shown). Differences in the signs of the two stability estimates are more common in Fig. 5b (12.4%) than in 5a (1.5%). This may be due to the selection of ε for calculating θ_0, since it is possible that ε changes slightly with changing surface conditions; an added measurement uncertainty which does not occur in the temperature measurements at 2 m.

$Ri_{B,2/10}$ in Fig. 5a follows Eqn. 10 fairly well on the unstable side, while in Fig. 5b $Ri_{B,S/10}$ is closer to Eqn. 9. On the stable side, $Ri_{B,S/10}$ agrees better with Eqn. 8 than $Ri_{B,2/10}$ although the measurements indicate more neutral stratification than the theoretical relationship would imply. It should also be noted that Fig. 5 shows some values outside the suggested limitations of Eqns. 8–10.

It is clear from Fig. 5 that the method Ri_B is determined by (i.e., which heights are used) has a great impact on the results. Since z/L needs to be determined from Ri_B both in the GM and the BM, different relations might be necessary depending on which measurement heights are employed.

Citation: *Polar Research* 2014, *33*, 21567, http://dx.doi.org/10.3402/polar.v33.21567

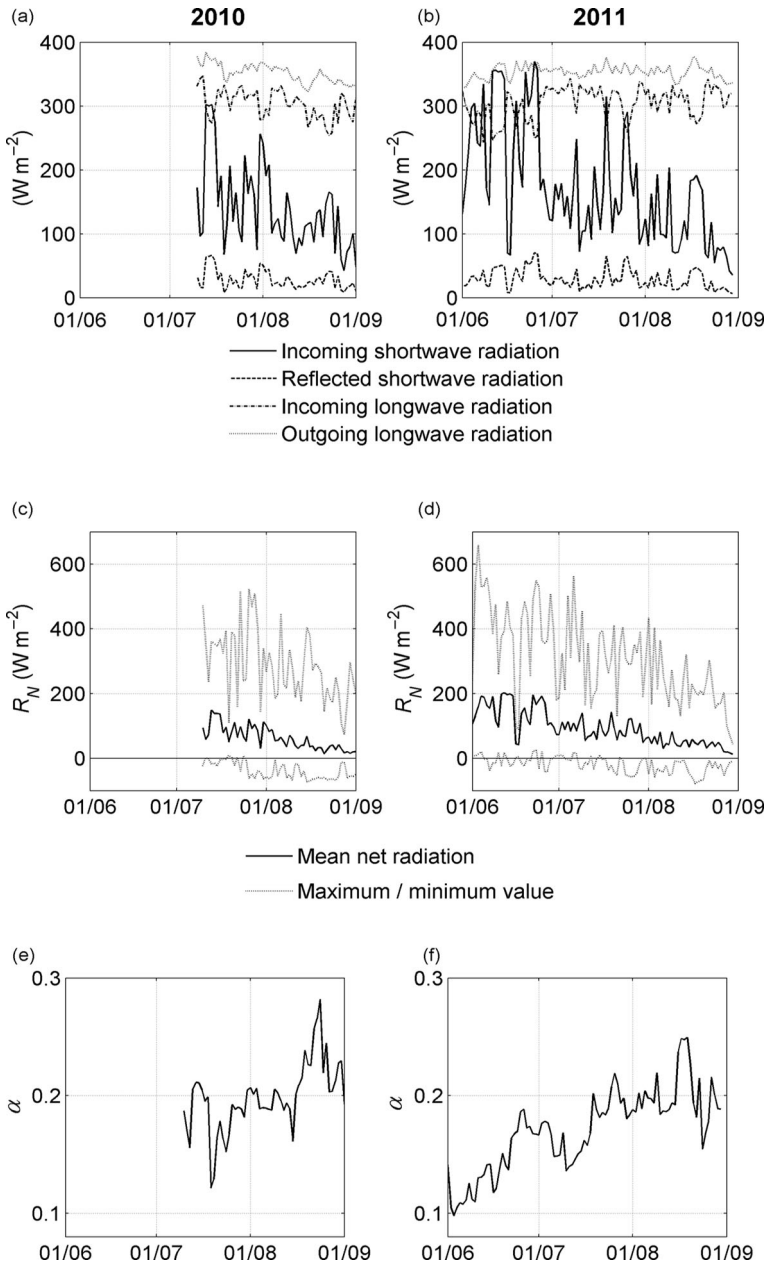

Fig. 3 Overview of daily means of radiation parameters: (a) the four components of radiation in 2010 and (b) in 2011; (c) net radiation (R_N) in 2010 and (d) in 2011; and (e) albedo (α) in 2010 and (f) in 2011.

This may explain why separate authors have recommended different relationships between Ri and z/L. On the other hand, here, Ri_B has been used for the comparison, and not Ri (Eqn. 4), which might increase the errors slightly as well.

Roughness

z_0 has been calculated in two ways: according to Eqn. 11 (Fig. 6a, c), using data from the sonic anemometer; and according to Eqn. 12 (Fig. 6b, d), using data from the slow-response instruments (2 and 10 m). Only near-neutral data are shown, $-0.025 < z/L < 0.025$ (Fig. 6a, c), $-0.025 < Ri_{B,2/10} < 0.025$ (Fig. 6b, d); changing these limits has little impact on the scatter.

Both methods show similar results, with z_0 mostly varying between $1{\cdot}10^{-4}$ and $2{\cdot}10^{-2}$ m. There is a clear dependency of z_0 on the wind direction and major changes occur with only small variation in wind direction despite the fetch conditions being visually similar in all considered

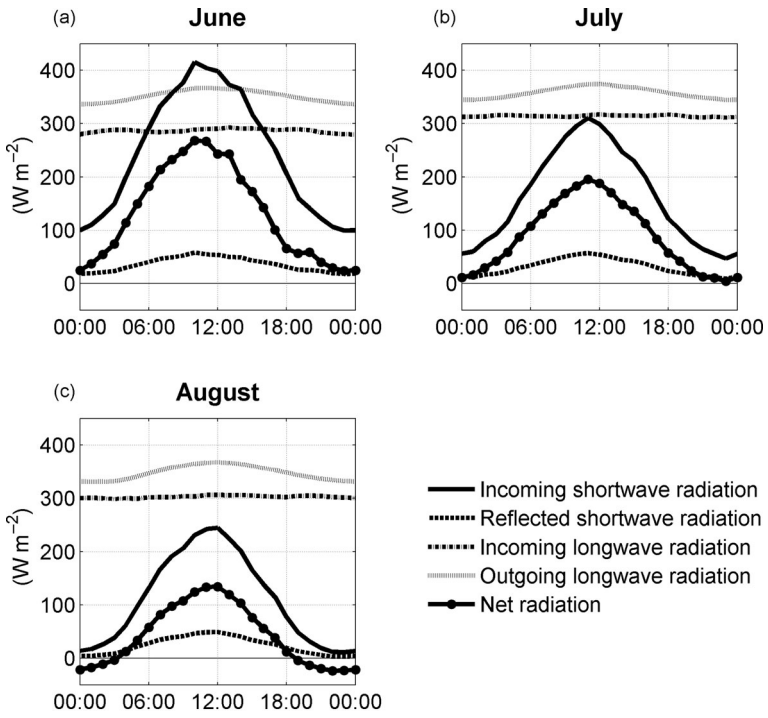

Fig. 4 Daily radiation budget for (a) June, (b) July and (c) August.

directions. Figure 6a and b also show that there are two dominating wind directions in Adventdalen, in (90–160°) or out the valley (270–350°). A few data points are from wind coming from one of the side valleys in Adventdalen (approximately 215°). There is also a dependency of U_{10} (Fig. 6c, d), although not as clear as for the wind direction.

To determine one single z_0 for the measurement site in Adventdalen is consequently difficult. In the following calculations $z_0 = 3.5 \cdot 10^{-3}$ m has been used, which is the median value of the measured z_0. This is close to the z_0 ($3.0 \cdot 10^{-3}$ m) Lloyd et al. (2001) found for a similar site in Ny-Ålesund.

Turbulent fluxes of momentum and heat

τ and H_S have been determined using the ECM, the GM and the BM. In addition, H_L has been estimated using the GM. For the ECM, the sonic anemometer data was used and B has been determined from the slow-response instruments. The difference between the uncorrected sensible heat flux and the corrected H_S (using Eqn. 14)

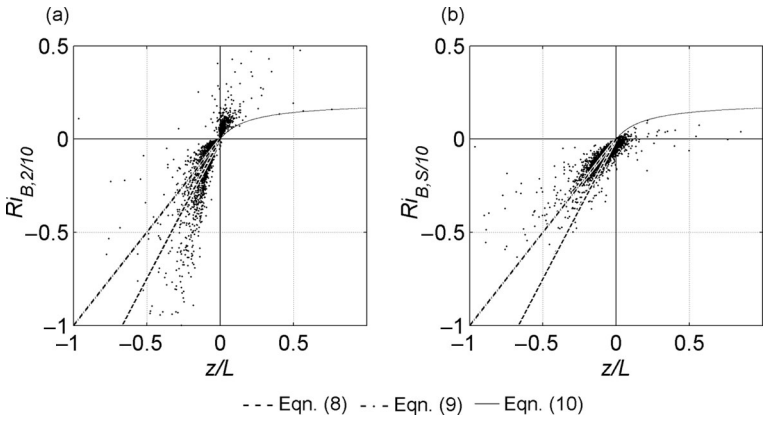

Fig. 5 Comparison of the bulk Richardson number (Ri_B) and z/L: (a) Ri_B between 2 and 10 m; (b) Ri_B between the surface and 10 m.

Citation: *Polar Research* 2014, *33*, 21567, http://dx.doi.org/10.3402/polar.v33.21567

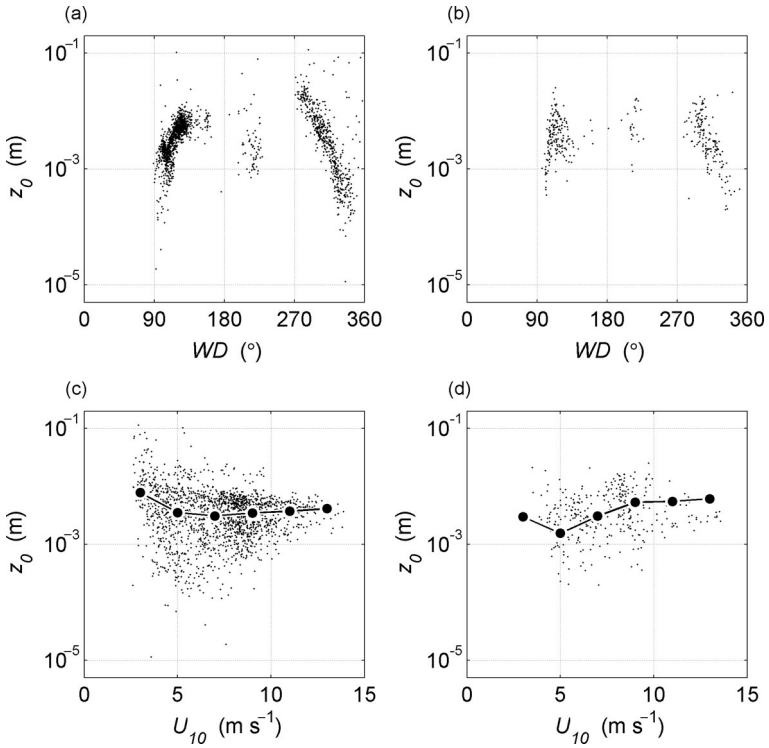

Fig. 6 The aerodynamic roughness length (z_0) calculated for near neutral values, in (a) and (c) using sonic anemometer data ($-0.025 < z/L < 0.025$) with Eqn. 11 and in (b) and (d) using slow-response measurements ($-0.025 < Ri_{B,2/10} < 0.025$) with Eqn. 12. (a) and (b) show z_0 as a function of wind direction (*WD*) and (c) and (d) as a function of the wind speed at 10 m (U_{10}), where median values for each 2.5 m s^{-1} are also shown (large filled circles).

is very small; H_S being larger by usually only a few W m^{-2} (not shown). The same small difference was found in Sjöblom (2010), where H_S was measured directly with a fine wire thermocouple in Adventdalen. This suggests that the correction in Eqn. 14 is adequate for these conditions.

For the GM, the slow-response instruments at 2 and 10 m have been used. z/L was determined from Eqn. 10 on the unstable side and from Eqn. 8 on the stable side. q in Eqn. 21 was calculated from the relative humidity employing standard relationships.

The slow-response instruments at 10 m (temperature and relative humidity recalculated from 9 to 10 m) were also used in the BM, together with θ_0 determined from Eqn. 3 and $\varepsilon = 0.97$. In addition, z_0 and z_{0T} have to be given values. As described earlier, $z_0 = 3.5 \cdot 10^{-3}$ m was chosen, and z_{0T} was set to 10% of z_0, in accordance with Foken (2008), that is, $3.5 \cdot 10^{-4}$ m. z/L was calculated from $Ri_{B,S/10}$ and Eqn. 9 on the unstable side and Eqn. 8 on the stable side. When interpreting the results for all three methods, it should be remembered that data with, for example small U and small vertical temperature differences, have been removed.

Figure 7a–d compares τ and H_S from the GM and the BM against the ECM. Although the scatter is relatively great, the GM works well, especially for τ, where the GM is only 5% higher than the ECM on average. For H_S, the GM is 40% lower than the ECM on the unstable side and on the stable side H_S is 67% higher in magnitude. This seems like a large difference, but keeping in mind that the magnitudes of H_S are small, the actual difference between the two methods is only about 20 W m^{-2} on the unstable side and 12 W m^{-2} on the stable. Less than 0.4% of H_S have different signs for the two methods.

The BM, on the other hand, overestimates the magnitude of both τ and H_S. For high H_S, the BM gives more than twice as large values as the ECM. There are also many cases (7.3%) where the ECM and the BM have different signs of H_S. On average, τ is 74% higher with the BM than the ECM, and ignoring data with different signs, H_S is 161% higher in magnitude on the unstable side, but only 11% on the stable side, which corresponds to approximately 75 and 3 W m^{-2}, respectively.

Since there is an obvious bias in the BM, the question is if the method can be easily adjusted to gain a better correspondence to the ECM. As discussed earlier, determining one z_0 for Adventdalen is difficult and therefore different z_0 were tested in the BM calculations. In Fig. 7e, f, a value of $z_0 = 5 \cdot 10^{-4}$ m (z_{0T} still 10% of z_0) was applied. The BM and the ECM now agree much better,

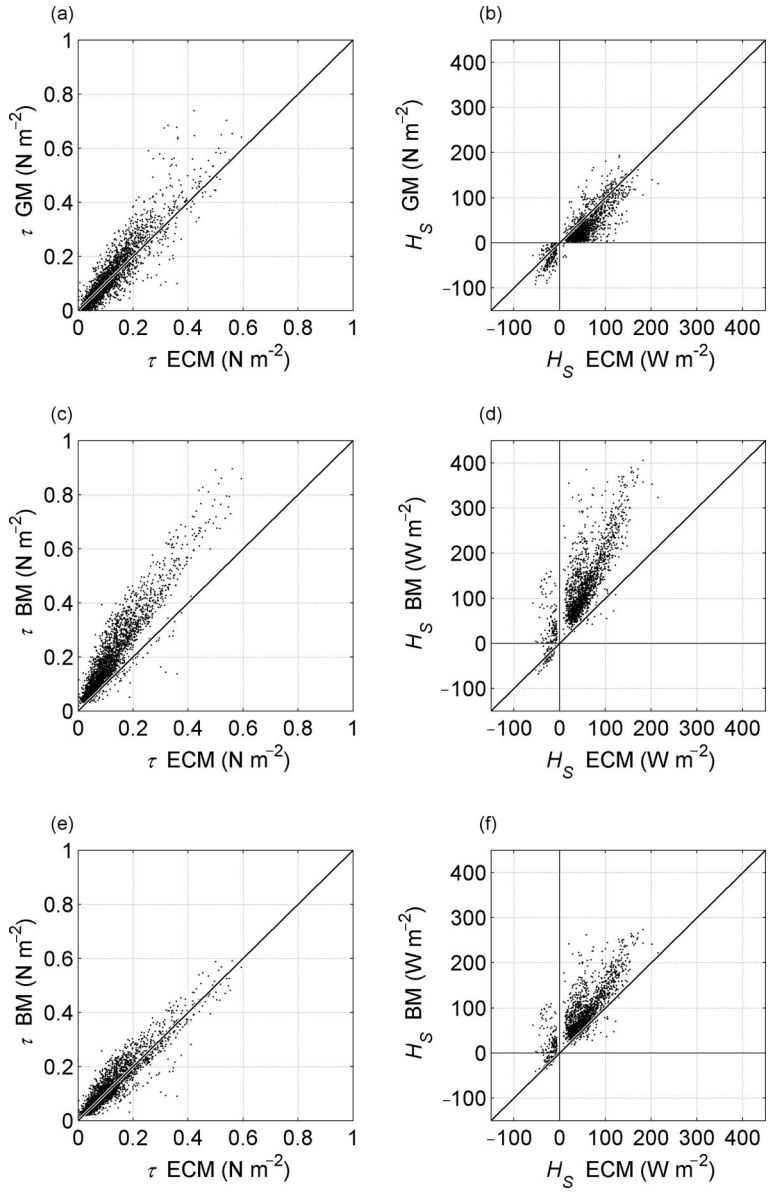

Fig. 7 Comparison of different methods to calculate momentum flux (τ) and sensible heat flux (H_s): (a) and (b) plot of the eddy covariance method (ECM) against the gradient method (GM); (c) and (d) plot of the ECM against the bulk method (BM); (e) and (f) plot of the ECM against a modified BM, as described in the text.

especially for τ, where the overestimation is 13% on average. H_S from the BM still gives too high values on the unstable side (77% or 35 W m^{-2} higher), while on the stable side the BM now has 22% lower magnitude than the ECM on average (or 5 W m^{-2}), that is, slightly worse after the modification. The problem with different signs in the ECM and the BM also still exists. However, a z_0 of $5{\cdot}10^{-4}$ m is far too low as an average value when looking at Fig. 6, and according to Arya (2001), it would resemble a surface of a flat desert, that is, this is purely a fictional value. Moreover, it shows that the BM is especially sensitive to the choice of z_0. Hence, results using this method should be interpreted with caution as they are very dependent on the initial values, not only of z_0, but also of z_{0T} and ε, which has not been discussed in detail here.

In Fig. 8, the time series of H_S (Fig. 8a–d) and H_L (Fig. 8e, f) for the two years are shown (Fig. 8a and b are determined from the ECM and Fig. 8c–f from the GM). H_S from the ECM and the GM follow each other well, although similar to Fig. 7, the ECM generally gives higher values. As expected, H_S is usually positive with the

Citation: *Polar Research* 2014, *33*, 21567, http://dx.doi.org/10.3402/polar.v33.21567

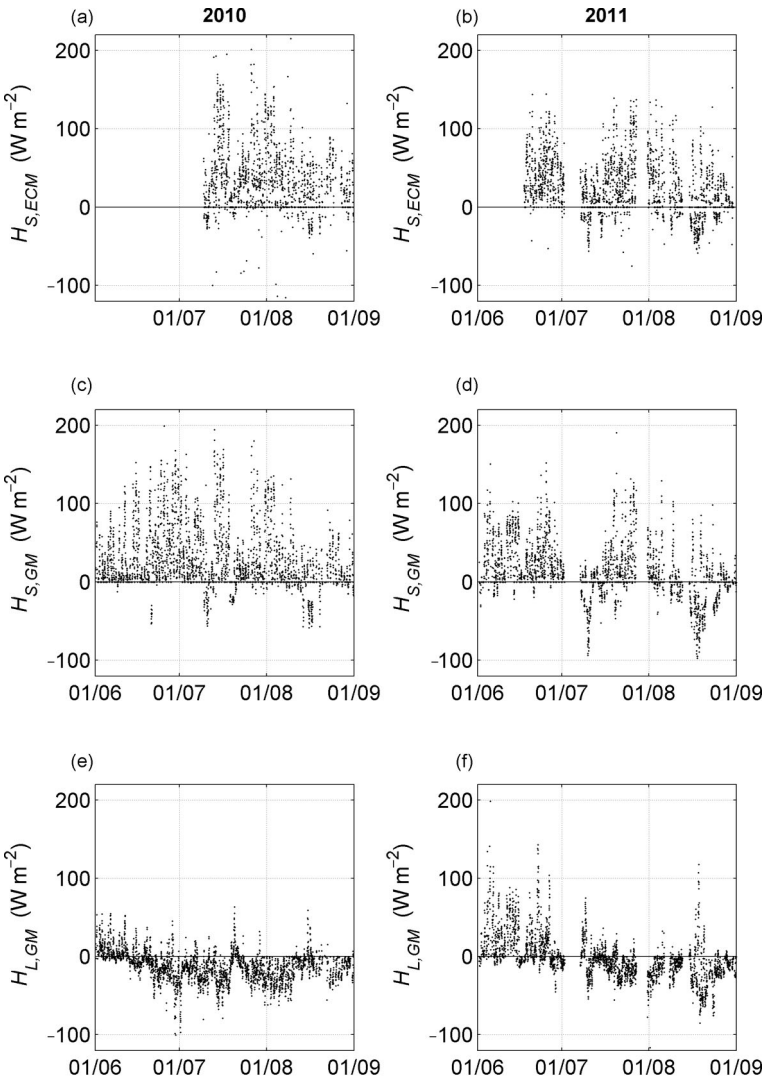

Fig. 8 Time series for 2010 and 2011: (a) and (b) show the sensible heat flux (H_s) calculated with the eddy covariance method and (c) and (d) with the gradient method. In (e) and (f) the latent heat flux (H_L) from the gradient method is shown.

greatest values in June and July, which can also be seen in Table 1, where monthly mean values from the different methods are given. What is more unusual is that H_L changes sign from positive to negative during the summer. Harding & Lloyd (1998), Lloyd et al. (2001) and Westermann et al. (2009) found that H_L is constantly positive during the summer in Ny-Ålesund, Svalbard, but in Adventdalen this changes through the summer. The same pattern can be seen for both years, with H_L positive in early June, and a change in sign in late June; the decrease continuing in July and August. This is likely to be the result of the active layer of the permafrost in Adventdalen drying fast after the snow melts, hence the evaporation from the soil surface decreases and the transport of moisture instead becomes downward. In addition, low stratus clouds are common in Adventdalen in July and August, which might enhance this downward transport. Moreover, compared to Ny-Ålesund, Adventdalen has considerably less precipitation on average, 51 mm compared to 84 mm in June–August and both summers of 2010 and 2011 were also drier than average, with only about 50% of the normal precipitation in this area.

Surface energy budget

By using the GM and the radiation measurements, all components in the SEB (Eqn. 30) can be determined, except H_G, which can be seen as the residual. Figure 9 shows the average SEB for 24-h for three months, respectively. For comparison, H_S from the ECM

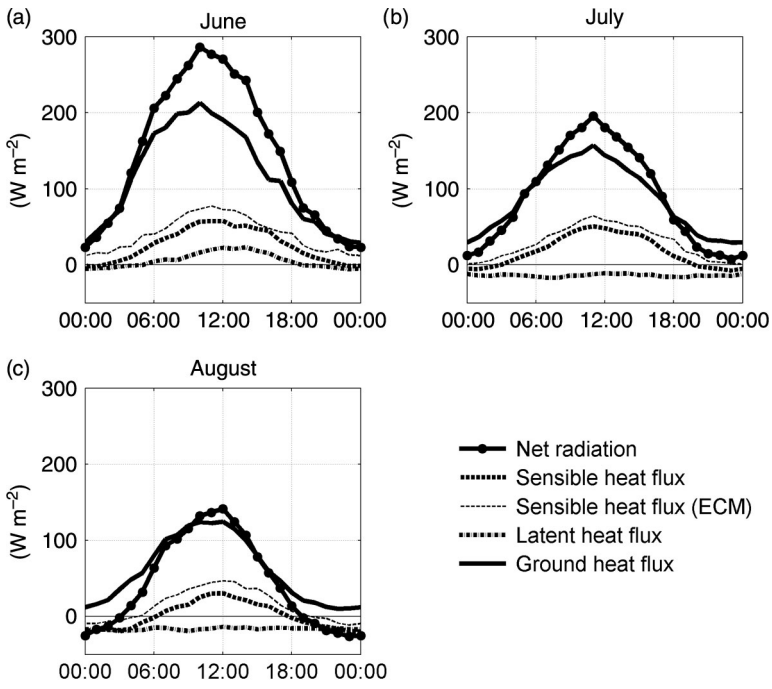

Fig. 9 Daily surface energy budget (SEB) for (a) June, (b) July and (c) August. For comparison, the sensible heat flux from the eddy covariance method (ECM) is shown.

is also shown. Similar to Fig. 4, the data used in Fig. 9a are limited due to the late start of the field campaign in 2010.

As discussed earlier, R_N decreases through the summer, but on average remains positive except during some hours during night in August, when it falls to approximately -25 W m^{-2}. H_S has a diurnal variation although the values are generally small. The greatest values occur during daytime with approximately 55, 50 and 30 W m^{-2} for the three months, respectively. In June, H_S is close to zero during the night and becomes slightly negative in July and August (about -15 W m^{-2}). H_L follows the same pattern as H_S in June, although with a smaller magnitude, but as shown in Fig. 8, H_L becomes constantly negative in July and August, varying between -25 and -5 W m^{-2}.

Since H_G is a residual it will also contain all the errors from the other fluxes, which means the results should be interpreted with caution. Performing a simple sensitivity analysis, where the instrument accuracies for radiation, wind speed, temperature and relative humidity are taken into account shows that the possible error is largest in June with an average of approximately $\pm 40\%$, while the error in July is $\pm 20\%$ and in August about $\pm 7\%$. Despite this, it is interesting that H_G is positive for all three months, including during the night (even when the instrument accuracies are taken into account), when the negative H_S and H_L will contribute to the warming of the surface.

It should again be remembered that some data have been discarded which might have an influence on the precise magnitudes of H_S and H_L. It was also shown earlier that H_S calculated with the GM and the ECM shows a difference which ought to be taken into account as well. Nevertheless, the trends are still clear.

Discussion and conclusions

Two observation techniques for turbulent momentum and sensible heat fluxes, the GM and the BM, using comparatively robust instrumentation with low power consumption, were tested in a High-Arctic valley in Svalbard for two consecutive snow-free summers and compared against the more direct ECM.

The GM gives the best results of the two techniques when compared to the ECM. τ agrees within 5%; H_S is approximately 40% lower (or 20 W m^{-2}) for unstable conditions and 67% higher (or 12 W m^{-2}) for stable conditions. The GM only has a few cases (less than 0.4%) with different sign of H_S from the ECM. Further advantages with the GM are that it only needs meteorological measurements at two arbitrary levels, no surface measurements are needed and it relies on fewer assumptions than the BM.

The BM, in contrast, has a clear bias, both for τ and H_S and there are several instances (7.3% of the data) where H_S has a different sign between the BM and the ECM.

Citation: *Polar Research* 2014, *33*, 21567, http://dx.doi.org/10.3402/polar.v33.21567

Adjusting z_0 to an unrealistic value makes the agreement better, especially for τ, but H_S still has too high values for unstable stratification and it becomes slightly worse for stable stratification. Hence, the BM is very sensitive to the choice of z_0, which can be difficult to determine. Even in a wide valley as Adventdalen where the surface appears to be fairly homogeneous in the flux footprint area, z_0 has a clear dependency on the wind direction. In addition to z_0, z_{0T} has to be determined for calculations of H_S. Here it was assumed that z_{0T} was 10% of z_0 but, as Mahrt & Vickers (2004) suggest, the results from the BM may be influenced by how z_{0T} was determined. Although only one level of meteorological observations is required, the BM also needs measurements at the surface. Over land, θ_0 can be determined through the longwave radiation, but ε has to be known. To decide q at the surface is usually possible over water where a saturated surface can be assumed, but over land it is more difficult. U, however, can be assumed to be zero at the surface.

Nevertheless, both the GM and the BM are not direct methods and both rely on assumptions and a correct representation of the Monin-Obukhov similarity theory. The parameterizations have limited stability ranges that have not been taken into account here and which add to the uncertainty of the results. Any data from slow-response instruments should also be treated with caution, especially if the instruments are of the more robust type. The accuracy of these instruments is often not great and if the gradient between the two levels is too small, the data cannot be used. This means that low fluxes are naturally filtered out, which will influence the results to some degree. Also, using naturally ventilated temperature and humidity sensors, which is common when low power consumption is required, can in some cases, especially in slow wind conditions or during strong radiative flux, have a significant influence on the readings (e.g., Kurzeja 2010). Hence, if the wind speed is too low, neither the anemometers nor the other sensors will give reliable readings. Moreover, Lüer & Bareiss (2010) concluded after testing the BM over snow that inversion layers close to the ground, that is, below the lowest measuring level, can lead to erroneous Ri_B, which in turn leads to incorrect fluxes. How Ri is determined from the observations might also have an influence on the results.

In addition to testing the observation techniques, the radiation budget and the SEB have been presented. α increases from approximately 0.1 to 0.2 over the summer. This shows that the ground surface is drying throughout the summer, which also has an effect on the turbulent fluxes. In particular, H_L changes significantly during the summer, from being positive in June to becoming negative in July and August. This is quite unusual since it is most common over tundra in the High Arctic to have positive H_L in the summer (e.g., Eugster et al. 2000; Westermann et al. 2009). The opposite signs of H_S and H_L during daytime in July and August suggest that most of the R_N goes into warming the grounds active layer through H_G. However, the precise values of H_G should be treated with caution since H_S and H_L are determined by the GM and H_G is a residual, thereby also containing the errors from the other estimates.

That the results from Adventdalen show a different SEB compared to similar places in the High Arctic adds to the fact that small-scale processes are very local in polar regions during summer and that more research and measurements are needed in order to understand what controls these processes. It is also important to understand what makes them different from similar processes further south.

To conclude, observations of turbulent fluxes of momentum and heat can be done with relatively cheap and robust instrumentation with low power consumption. However, caution should be taken in choice of technique and also in how the results are interpreted since the method itself can influence the actual results. Moreover, parameters such as z_0 and the SEB show a very local character which needs to be taken into account if the understanding of the High Arctic and the climate system as a whole is to improve.

Acknowledgements

Prof. S. J. Coulson is thanked for help with the measurements and valuable comments on the manuscript. This work was part of the CRYOMET—Bridging Models for the Terrestrial Cryosphere and the Atmosphere project (grant no. 2114465/V30), which is financed by the Norwegian Research Council.

References

AMAP (Arctic Monitoring and Assessment Programme) 2011. *Snow, water, ice and permafrost in the Arctic (SWIPA): climate change and the cryosphere*. Oslo: Arctic Monitoring and Assessment Programme.

Andreas E.L., Horst T.W., Grachev A.A., Persson P.O.G., Fairall C.W., Guest P.S. & Jordan R.E. 2010. Parameterizing turbulent exchange over summer sea ice and the marginal ice zone. *Quarterly Journal of the Royal Meteorological Society 136*, 927–943.

Andreas E.L., Persson P.O.G., Jordan R.E., Horst T.W., Guest P.S., Grachev A.A. & Fairall C.W. 2010. Parameterizing turbulent exchange over sea ice in winter. *Journal of Hydrometeorology 11*, 87–104.

Arya S.P. 2001. *Introduction to micrometeorology*. San Diego: Academic Press.

Ávila-Jiménez M.L., Coulson S.J., Solhøy T. & Sjöblom A. 2010. Overwintering of terrestrial Arctic arthropods: the fauna of Svalbard now and in the future. *Polar Research 29*, 127–137.

Boike J., Roth K. & Ippisch O. 2003. Seasonal snow cover on frozen ground: energy balance calculations of a permafrost site near Ny-Ålesund, Spitsbergen. *Journal of Geophysical Research—Atmospheres 108*, article no. 8163, doi: 10.1029/2001JD000939.

Brunke M.A., Zhou M., Zeng X. & Andreas E.L. 2006. An intercomparison of bulk aerodynamic algorithms used over sea ice with data from the Surface Heat Budget for the Arctic Ocean (SHEBA) experiment. *Journal of Geophysical Research—Oceans 111*, C09001, doi: 10.1029/2005JC002907.

Duynkerke P.G. & van den Broeke M.R. 1994. Surface energy balance and katabatic flow over glacier and tundra during GIMEX-91. *Global and Planetary Change 9*, 17–28.

Esau I., Argentini S., Przybylak R., Repina I. & Sjöblom A. 2012. Svalbard meteorology. *Advances in Meteorology 2012*, article no. 818473, doi: 10.1155/2012/818473.

Eugster W., Rouse W.R., Pielke SR R.A., McFadden J.P., Baldocchi D.D., Kittel T.G.F., Chapin F.S., III, Liston G.E., Vidale P.L., Vaganov E. & Chambers S. 2000. Land–atmosphere energy exchange in Arctic tundra and boreal forest: available data and feedbacks to climate. *Global Change Biology 6*, 84–115.

Foken T. 2008. *Micrometeorology*. Berlin: Springer.

Førland E.J., Benestad R., Hanssen-Bauer I., Haugen J.E. & Skaugen T.E. 2011. Temperature and precipitation development at Svalbard 1900–2100. *Advances in Meteorology 2011*, article no. 893790, doi: 10.1155/2011/893790.

Grachev A.A., Andreas E.L., Fairall C.W., Guest P.S. & Persson P.O.G. 2007. SHEBA flux–profile relationships in the stable atmospheric boundary layer. *Boundary-Layer Meteorology 124*, 315–333.

Grachev A.A., Andreas E.L., Fairall C.W., Guest P.S. & Persson P.O.G. 2008. Turbulent measurements in the stable atmospheric boundary layer during SHEBA: ten years after. *Acta Geophysica 56*, 142–166.

Harding R.J. & Lloyd C.R. 1998. Fluxes of water and energy from three high latitude tundra sites in Svalbard. *Nordic Hydrology 29*, 267–284.

Högström U. 1996. Review of some basic characteristics of the atmospheric surface layer. *Boundary-Layer Meteorology 78*, 215–246.

Kilpeläinen T., Vihma T. & Olafsson H. 2011. Modelling of spatial variability and topographic effects over Arctic fjords in Svalbard. *Tellus Series A 63*, 223–237.

Kral S.T., Sjöblom A. & Nygård T. 2014. Observations of summer turbulent surface fluxes in a High Arctic fjord. *Quarterly Journal of the Royal Meteorological Society 140*, 666–675.

Kurzeja R. 2010. Accurate temperature measurements in a naturally-aspirated radiation shield. *Boundary-Layer Meteorology 134*, 181–193.

Langer M.S., Westermann S., Muster S., Piel K. & Boike J. 2011. The surface energy balance of a polygonal tundra site in northern Siberia. Part 1: spring to fall. *The Cryopshere 5*, 151–171.

Lee X., Massman W. & Law B. 2004. *Handbook of micrometeorology, a guide for surface flux measurement and analysis*. Dordrecht: Kluwer Academic Publishers.

Lloyd C.R., Harding R.J., Friborg T. & Aurela M. 2001. Surface fluxes of heat and water vapour from sites in the European Arctic. *Theoretical and Applied Climatology 70*, 19–33.

Lüers J. & Bareiss J. 2010. The effect of misleading surface temperature estimations on the sensible heat fluxes at a High Arctic site—the Arctic Turbulence Experiment 2006 on Svalbard (ARCTEX-2006). *Atmospheric Chemistry and Physics 10*, 157–168.

Lumley J.L. & Panofsky H.A. 1964. *The structure of atmospheric turbulence*. New York: Interscience Publishers.

Lüpkes C., Gryanik V.M., Hartmann J. & Andreas E.L. 2012. A parameterization, based on sea ice morphology, of the neutral atmospheric drag coefficients for weather prediction and climate models. *Journal of Geophysical Research—Atmospheres 117*, D13112, doi: 10.1029/2012JD017630.

Lynch A.H., Chapin F.S. III, Hinzman L.D., Wu W., Lilly E., Vourlitis G. & Kim E. 1999. Surface energy balance on the Arctic tundra: measurements and models. *Journal of Climate 12*, 2585–2606.

Mahrt L. & Vickers D. 2004. Bulk formulation of the surface heat flux. *Boundary-Layer Meteorology 110*, 357–379.

McFadden J.P., Stuart Chapin III F. & Hollinger D.Y. 1998. Subgrid-scale variability in the surface energy balance of Arctic tundra. *Journal of Geophysical Research 103*, 28947–28961.

Niu X., Pinker R.T. & Cronin M.F. 2010. Radiative fluxes at high latitudes. *Geophysical Research Letters 37*, L20811, doi: 10.1029/2010GL044606.

Obukhov A.M. 1971. Turbulence in an atmosphere with a non-uniform temperature. *Boundary-Layer Meteorology 2*, 7–29.

Ohmura A. 1982. Climate and energy balance on the Arctic tundra. *Journal of Climatology 2*, 65–84.

Overland J.E., Wang M., Bond N.A., Walsh J.E., Kattsov V.M. & Chapman W.L. 2011. Considerations in the selection of global climate models for regional climate projections: the Arctic as a case study. *Journal of Climate 24*, 1583–1597.

Paulson C.A. 1970. The mathematical representation of wind speed and temperature profiles in the unstable atmospheric surface layer. *Journal of Applied Meteorology 9*, 857–861.

Persson P.O.G., Fairall C.W., Andreas E.L., Guest P.S. & Perovich D.K. 2002. Measurements near the atmospheric surface flux group tower at SHEBA: near-surface conditions and surface energy budget. *Journal of Geophysical Research—Oceans 107*, article no. 8045, doi: 10.1029/2000JC000705.

Rott H. & Obleitner F. 1992. The energy balance of dry tundra in west Greenland. *Arctic and Alpine Research 24*, 352–362.

Schotanus P., Nieuwstadt F.T.M. & De Bruin H.A.R. 1983. Temperature measurement with a sonic anemometer and

its application to heat and moisture fluxes. *Boundary-Layer Meteorology 26*, 81–93.

Sjöblom A. 2010. A solar eclipse seen from the High Arctic during the period of midnight sun: effects on the local meteorology. *Meteorology and Atmospheric Physics 107*, 123–136.

Sjöblom A. & Smedman A. 2002. The turbulent kinetic energy budget in the marine atmospheric surface layer. *Journal of Geophysical Research—Oceans 107*, article no. 3142, doi: 10.1029/2001JC001016.

Symon C., Arris L. & Heal B. (eds.) 2005. *Arctic climate impact assessment*. Cambridge: Cambridge University Press.

Vickers D. & Mahrt L. 1997. Quality control and sampling problems for tower and aircraft data. *Journal of Atmospheric and Oceanic Technology 14*, 512–526.

Walsh J.E., Overland J.E., Groisman P.Y. & Rudolf B. 2011. Ongoing climate change in the Arctic. *Ambio 40*, 6–16.

Wang M. & Overland J.E. 2012. A sea ice free summer Arctic within 30 years: an update from CMIP5 models. *Geophysical Research Letters 39*, L18501, doi: 10.1029/2012GL052868.

Westermann S., Langer M. & Boike J. 2011. Spatial and temporal variations of summer surface temperatures of High-Arctic tundra on Svalbard—implications for MODIS LST based permafrost monitoring. *Remote Sensing of Environment 115*, 908–922.

Westermann S., Lüers J., Langer M. & Boike J. 2009. The annual surface energy budget of a High-Arctic permafrost site on Svalbard, Norway. *The Cryosphere 3*, 345–263.

Winther J.-G., Godtliebsen F., Gerland S. & Isachsen P.E. 2002. Surface albedo in Ny-Ålesund, Svalbard: variability and trends during 1981–1997. *Global and Planetary Change 32*, 127–139.